

Laser microscopy of tunneling magnetoresistance in manganite grain-boundary junctions

M. Wagenknecht,¹ H. Eitel,¹ T. Nachtrab,¹ J. B. Philipp,² R. Gross,² R. Kleiner,¹ and D. Koelle^{1,*}

¹*Physikalisches Institut – Experimentalphysik II, Universität Tübingen,
Auf der Morgenstelle 14, D-72076 Tübingen, Germany*

²*Walther-Meissner-Institut, Bayerische Akademie der Wissenschaften,
Walther-Meissner-Str. 8, D-85748 Garching, Germany*

(Dated: November 24, 2018)

Using low-temperature scanning laser microscopy we directly image electric transport in a magnetoresistive element, a manganite thin film intersected by a grain boundary (GB). Imaging at variable temperature allows reconstruction and comparison of the local resistance vs temperature for both, the manganite film and the GB. Imaging at low temperature also shows that the GB switches between different resistive states due to the formation and growth of magnetic domains along the GB. We observe different types of domain wall growth; in most cases a domain wall nucleates at one edge of the bridge and then proceeds towards the other edge.

PACS numbers: 72.25.Mk, 75.47.Lx, 75.60.Ch, 75.70.-i

Doped perovskite manganites of composition $R_{1-x}A_xMnO_3$ (R: rare-earth, A: alkaline-earth element) have attracted renewed interest over the last years due to the interesting interplay between charge, spin, orbital and structural degrees of freedom[1]. This is related to ordering phenomena which lead *e.g.* to the colossal magnetoresistance (CMR) effect[2, 3] when a large magnetic field B in the Tesla-range is applied close to the Curie temperature T_C to align the magnetic moments of the Mn ions, which increases electric conductivity by up to several orders of magnitude. Moreover, at temperatures $T < T_C$ a substantial magnetoresistance (MR) in much lower fields (~ 10 mT) has been found in polycrystals and thin films with grain boundaries (GBs)[4, 5, 6]. Such a low-field MR effect allows switching by small magnetic fields between a low- and high-resistance state, characterized by parallel and antiparallel orientation of the magnetization of two ferromagnetic grains separated by a GB. This effect can be of considerable interest for applications like magnetic storage[7]. However, a thorough understanding of the magnetotransport properties in manganite GBs is still lacking, and the models, proposed to describe those properties are controversial. Whereas some suggest activated carrier transport within a defective region adjacent to the GB (with depressed magnetic order)[8], or transport through an interfacial depletion layer at an abrupt metal-semiconductor contact at the GB[9, 10], most of them are based on spin-polarized tunneling[11] between ferromagnetic grains through an insulating GB barrier[4], including *e.g.* resonant[12] or inelastic[13] tunneling via localized states in the barrier, which can be *e.g.* due to paramagnetic impurities[14] that may be magnetically ordered[15]. Most experiments were performed on well-defined, individual GB junctions or

junction arrays fabricated by epitaxial growth of manganite films on bicrystal substrates[6, 13, 16, 17, 18, 19]. Large low-field MR ratios up to 300% at $T=4.2$ K were found in individual $La_{2/3}Ca_{1/3}MnO_3$ (LCMO) GB junctions[17]. Based on the Julliere model for elastic spin polarized tunneling[20], such a large tunnelling magnetoresistance (TMR) effect can be achieved in materials with large spin polarization P . In this sense, the doped manganites are very promising materials for device applications due to their half-metallic nature with P close to unity[21]. Accordingly, high TMR ratios have been also found for trilayer spin valve devices using doped manganites[22, 23, 24].

Obviously, the magnetotransport properties of any TMR element are affected by the magnetization of the ferromagnetic electrodes close to the barrier, and in particular by magnetic domain formation and domain wall motion during field switching. Therefore, a better understanding of magnetotransport in GB junctions from doped manganites requires consideration of magnetic domains[17, 19, 25]. The measured TMR always represents an integral quantity obtained by averaging over the area of the tunnel junction. Both in view of applications and from a fundamental point of view it is of high interest to see how locally the TMR depends on the magnetic properties of the electrodes and on the way the magnetization is switched by a magnetic field. Here we show that low-temperature scanning laser microscopy (LTSLM) allows to locally detect the magnetoresistance of LCMO grain boundaries. Besides the more or less homogeneous high- and low-resistance states we also find intermediate states where low- and high-resistance regions coexist. Our investigations give insight into the magnetic domain formation near the grain boundary and its impact on the magnetoresistance of these devices.

To provide insight into the interplay between electric transport and magnetic domain formation, we studied GB junctions made from 80nm thick LCMO thin films, epitaxially grown by pulsed laser deposition on symmet-

*Electronic address: koelle@uni-tuebingen.de

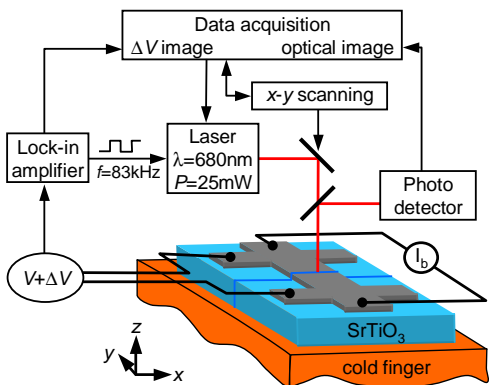


FIG. 1: (Color online) LTSLM setup: The sample is mounted on a cold finger; all other components are at 300 K. The laser beam is focused onto the LCMO microbridge at position (x_0, y_0) creating a hot spot ($\delta T \approx 3$ K, diam. $\sim 1.5 \mu\text{m}$). The local change in sample resistance induces a change ΔV of the globally measured voltage V , creating the electrical image $\Delta V(x_0, y_0)$. The reflected beam intensity vs. (x_0, y_0) produces an optical image.

ric [001] tilt SrTiO_3 bicrystals with 24° misorientation angle[17]. The films are patterned into $W = 30 \mu\text{m}$ wide bridges crossing the GB. Voltage pads separated by $L = 70 \mu\text{m}$ along the bridge allow 4-point measurements. The samples are mounted on a cold finger (at $5 \text{ K} \leq T \leq 300 \text{ K}$) inside a ^4He optical flow cryostat. A Helmholtz coil produces a magnetic field up to 35 mT in the (x, y) plane of the film, parallel to the GB (along x) for measurements of the integral resistance $R(T, B)$. For imaging, the beam of a 25 mW diode laser ($\lambda = 680 \text{ nm}$) is focused onto the film surface [cf. Fig.1]. At the beam position (x_0, y_0) the sample is locally heated by $\delta T(x_0, y_0) \approx 3 \text{ K}$ within an area of diameter $d \approx 1.5 \mu\text{m}$, approximately given by the laser spot size. This local hot spot changes the local resistance $\sim (\partial R/\partial T)|_{(x_0, y_0)} \cdot \delta T(x_0, y_0)$, which induces a change of R and consequently a change $\Delta V(x_0, y_0) \propto I_b \cdot (\partial R/\partial T)|_{(x_0, y_0)} \cdot \delta T(x_0, y_0)$ of the total voltage V across the current biased bridge. Typically, ΔV is of order 1-20 μV , for a bias current $I_b = 5 \mu\text{A}$ (used for all measurements discussed below), and much larger than the thermoelectric voltage change ΔV_{th} ($I_b = 0$) [26, 27] in our samples. To improve the signal-to-noise ratio, we blank the laser beam at a frequency $f = 83 \text{ kHz}$ and detect ΔV with a lock-in technique. An electrical image is obtained by monitoring $\Delta V(x_0, y_0)$. Simultaneously we detect the reflected beam intensity vs. (x_0, y_0) to obtain an optical image of the scanned surface. We investigated two different LCMO bridges intersected by a GB which showed qualitatively the same behavior. Below we present data obtained on one of those bridges.

Fig.2(a) shows $R(T)$ in zero field (zfc) and in $B = 10 \text{ mT}$ (fc). At $T = 220 \text{ K}$ the film undergoes a metal-to-insulator transition leading to the well known high-field CMR[2, 28]. At $T < 150 \text{ K}$ the fc- and zfc-curves differ,

i.e. the TMR of the GB appears. We attribute the high-resistance state to antiparallel and the low-resistance state to parallel orientation of the magnetization of the LCMO films adjacent to the GB. The relative orientation of the magnetization vectors can be flipped between parallel and antiparallel by sweeping B at low T , as indicated in the inset of Fig.2(a), showing switching between low- and high-resistance state. Fig.2(b) shows the T -dependence of the high- and low-resistance state for $10 \text{ K} < T < 100 \text{ K}$. Note that, at a given temperature, dR/dT differs for the two states. As the LTSLM signal $\Delta V(x_0, y_0)$ changes sign with $(\partial R/\partial T)|_{(x_0, y_0)}$ this observation is consistent with the LTSLM images of the GB [see insets of Fig.2(b)] taken for each of the two states at three different temperatures. Indeed, in all cases the ΔV signal obtained along the GB turned out to be proportional to dR/dT , which thus can be considered as the quantity we primarily measure locally. In particular, at

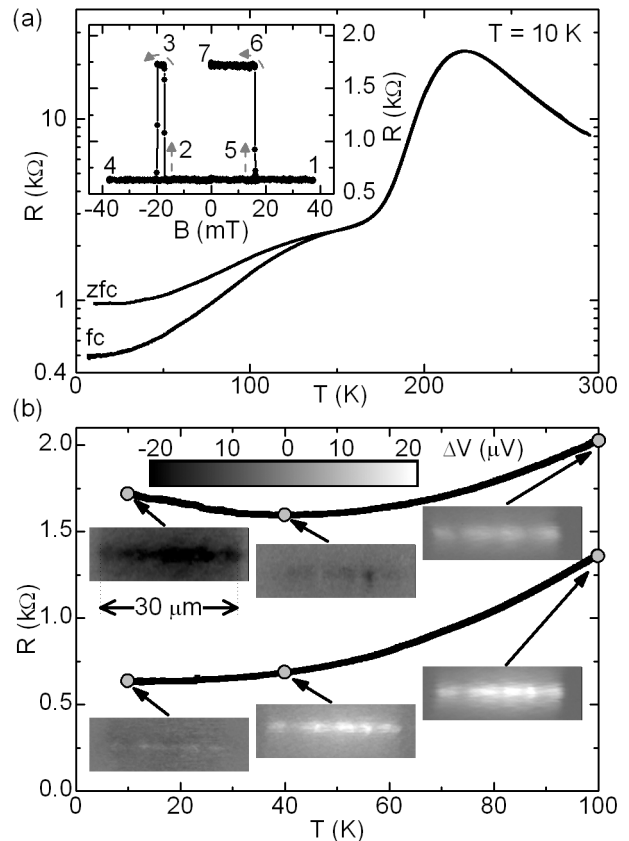


FIG. 2: TMR effect of LCMO bridge intersected by a grain boundary ($I_b = 5 \mu\text{A}$; B is in-plane and parallel to the GB). (a) $R(T)$ obtained by cooling in zero field (zfc) and in $B = 10 \text{ mT}$ (fc). Inset: $R(B)$ at $T = 10 \text{ K}$. R switches between antiparallel (high-resistance state) and parallel (low-resistance state) magnetization of the LCMO films adjacent to the GB by sweeping B (from 1 to 7, as indicated by dashed arrows). (b) $R(T)$ for high- and low-resistance state at $B = 0$. Insets show LTSLM ΔV images for both states taken at different T ; upper inset shows ΔV scale.

the lowest temperature $T = 10$ K, dR/dT vanishes in the low-resistance state and is negative in the high-resistance state [29]. Accordingly, the ΔV signal at the GB is vanishing in the low-resistance state and is negative in the high-resistance state. This fact allows discrimination by LTSLM imaging of regions along the GB with parallel and antiparallel orientation of the magnetization of the grains separated by the GB, as will be discussed below. Further note, that in each ΔV image, the contrast varies along the GB, indicating that the GB is not completely homogeneous. This can be attributed to inhomogeneities (i) in the surface morphology, causing a small variation of the absorbed laser intensity, and (ii) in the microstructure of the film close to the GB, which can induce inhomogeneities in the tunnel barrier formed along the GB.

The ΔV images in Fig.2(b) clearly show the absence of any signal from the manganite film (above and below the GB) with total resistance R_{film} , consistent with $(dR_{film}/dT) \ll (dR_{GB}/dT)$ at $T \leq 100$ K. Hence, at low T , only properties of the GB are probed by laser imaging. This situation changes at higher T , in particular close to T_C . In the following, we demonstrate that LTSLM allows discrimination of the contributions from the film resistance R_{film} and the GB resistance R_{GB} to the overall resistance $R = R_{film} + R_{GB}$. From ΔV images taken at different T , we obtain the evolution of dR_{film}/dT and dR_{GB}/dT vs. T , and by integration over T we can reconstruct the local $R_{film}(T)$ and $R_{GB}(T)$ curves.

For the following procedure the low resistance state was chosen. From ΔV images we calculated the average voltage signal $\Delta V(y_0) = W^{-1} \int \Delta V(x_0, y_0) dx_0$ for linescans ($y_0 = \text{const.}$) along the GB (ΔV_{GB}^*) and along a representative section of the bridge (ΔV_{film}), $\sim 20 \mu\text{m}$ above the GB. As the laser spot diameter is much larger than the GB width (few nm), the signal ΔV_{GB}^* contains a contribution from the film (for $T > 100$ K). To restore the "pure" GB signal for all values of T , we thus take $\Delta V_{GB} = \Delta V_{GB}^* - \Delta V_{film}$ to obtain $(dR_{GB}/dT)(T) \propto \Delta V_{GB}(T)$ and $(dR_{film}/dT)(T) \propto \Delta V_{film}(T)$. Due to the finite spot size d , the signal ΔV_{film} corresponds to a fraction d/L of the bridge of length $L = 70 \mu\text{m}$. Hence, we expect the overall resistance R and the LTSLM signals to be related as $(dR/dT) \propto \Delta V_{GB} + (L/d)\Delta V_{film} \equiv \Delta V_{eff}$. Fig.3 shows $\Delta V_{eff}(T)$ as obtained from LTSLM images (with $L/d = 50$), and for comparison, $(dR/dT)(T)$ as obtained from the integral $R(T)$ curve. With an effective spot size $d = L/50 = 1.4 \mu\text{m}$ we find excellent agreement between both curves over the whole temperature range. This proves on the one hand that the LTSLM signal is indeed of purely thermal origin. On the other hand, the knowledge of the effective spot size allows calculation of $\delta T(x_0, y_0)$, which turns out to be ≈ 3 K.

The inset of Fig.3 shows the local $R(T)$ curves, for both the film and the GB, as obtained from integration of the LTSLM voltage signals over T . The summation of both curves coincides reasonably well with the integral $R(T)$ curve. Deviations are most likely due to inhomogeneities in the bridge, which we neglected in the analysis of the LTSLM signals.

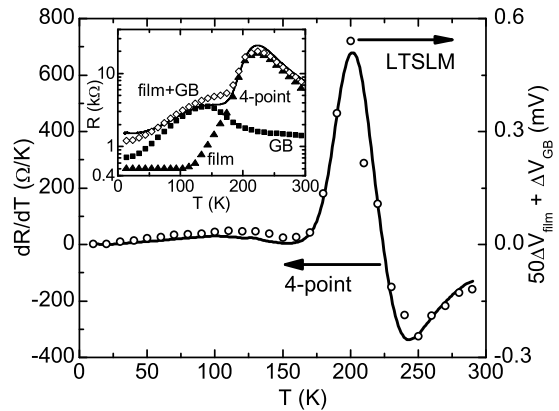


FIG. 3: T -dependence of LTSLM voltage signals (open dots) and comparison with integral $(dR/dT)(T)$ curve (solid line). Inset: Local $R(T)$ curves, reconstructed from integration of the LTSLM signals over T . The spatial resolution of LTSLM allows separation of the film (solid triangles) and GB (solid squares) resistances. The sum of both contributions (open diamonds) gives reasonably good agreement with the overall resistance of the bridge (solid line) measured by a conventional four point technique.

geneities in the bridge, which we neglected in the analysis of the LTSLM signals. The manganite film shows the well known metal-insulator transition near T_C (~ 220 K), and a relatively small (few 100Ω) T -independent resistance at $T \leq 110$ K. In this low- T regime, the GB resistance clearly dominates the overall bridge resistance and increases with T up to a maximum value of a few $k\Omega$ at $T \approx 140$ K, approximately at the same temperature where the low-field TMR effect disappears. This increase in R_{GB} with T is consistent with a decreasing magnetic order at the GB. Above 140 K, however, R_{GB} decreases again with further increasing T , which could be *e.g.* attributed to a thermally activated hopping mechanism dominating the transport across the GB at higher T in the paramagnetic regime. Interestingly, the maximum in R_{GB} appears at a temperature which is close to the onset temperature of increasing film resistance. A similar observation has been reported in Ref.[6]. Finally, we note that the GB resistance remains at a relatively high level even for temperatures above T_C . This gives strong evidence that the GB behaves as a tunnel barrier also in the paramagnetic phase of the manganite film, suggesting a tunneling transport mechanism.

So far, we considered only the high- and low-resistance states, with corresponding resistances R_{max} and R_{min} , respectively. However, intermediate-resistance states ($R_{min} < R < R_{max}$) can also be stabilized by properly sweeping B , as shown in Fig.4(a) for $T=10$ K. The corresponding LTSLM images show a striking change in the contrast along the GB. One section of normalized length $h \equiv H/W$ along the GB is in the high-resistance state ($\Delta V < 0$) while the other part is in the low-resistance state ($\Delta V \approx 0$). Defining the relative TMR

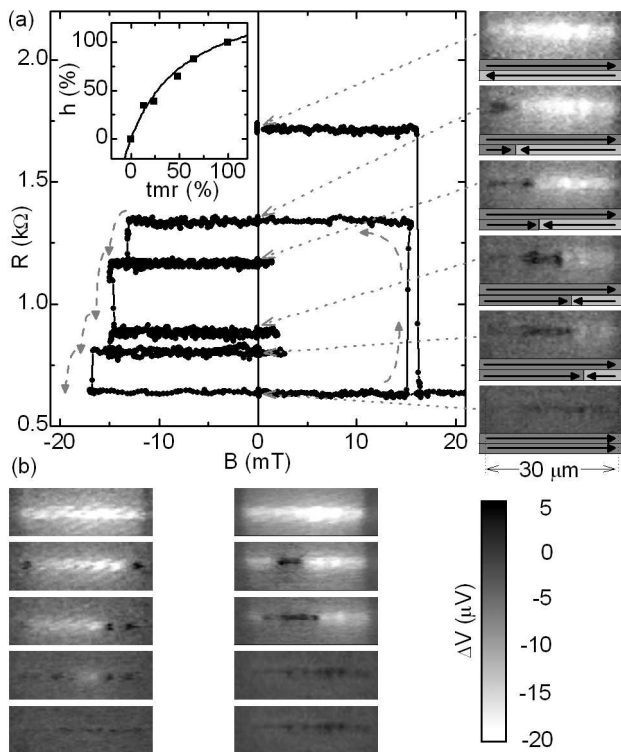


FIG. 4: Transition of LCMO GB junction from high- to low-resistance state by domain wall motion ($T=10\text{ K}$; $I_b = 5\ \mu\text{A}$). (a) $R(B)$ showing intermediate-resistance states (dashed arrows indicate field sweep direction). LTSLM images show separation of the GB into regions of high- and low-resistance states (dotted arrows mark bias points on $R(B)$). Consequently, one of the electrodes must have developed a magnetic domain boundary which nucleates at the left edge and moves along the GB to the right edge, as R is decreasing (arrows indicate schematically magnetization directions above and below GB). Inset: Fraction h of GB in high-resistance state vs relative TMR ratio; experiment (squares) and calculation (line). (b) LTSLM images showing two different transitions from the high- (top) to the low-resistance state (bottom). Left column: domain wall nucleation at both edges; right column: nucleation in the interior of the bridge.

ratio as $\text{tmr} \equiv (R - R_{\min})(R_{\max} - R_{\min})$ we can plot $h(\text{tmr})$ as obtained from LTSLM images and $R(B)$ data [c.f. inset of Fig.4(a)]. From our interpretation of the LTSLM signals it follows that $h(\text{tmr})$ should scale as $h(\text{tmr}) = \text{tmr} \cdot r_{\max} / \{1 + \text{tmr} \cdot (r_{\max} - 1)\}$, if we neglect R_{film} , with $r_{\max} \equiv R_{\max}/R_{\min}$. This relation is also shown in the inset of Fig.4(a) (as solid line). The good

agreement of experimental data and calculated $h(\text{tmr})$ supports our interpretation that LTSLM directly probes the TMR. The LTSLM images reveal the relative orientation of the magnetization of the LCMO films on both sides of the GB. Hence, one of the LCMO electrodes must have developed a domain boundary where the magnetization flips. However, we do not know how far the domain walls continue into the LCMO films. Such complementary information could be *e.g.* obtained by Kerr microscopy, which, however, requires smooth and highly reflective surfaces in contrast to LTSLM. How reproducible are the above results? We performed measurements as in Fig.4 for two samples and about 20 times, also at various T . In most cases we found nucleation of a domain wall at one edge of the GB which then proceeds towards the other edge [cf. Fig.4(a)]. For the sample discussed here, in seven out of ten measurements at 10K we found domain wall nucleation at one edge. In two cases we found domain wall nucleation at both edges [cf. Fig.4(b), left column], and only in one case a domain nucleated in the interior of the bridge [Fig.4(b), right column]. This process occurs more rarely, because it requires simultaneous creation of two domain walls, which is energetically less favorable than producing seed domains at the edges of the GB.

In conclusion, we demonstrated spatially resolved detection of the TMR of LCMO grain boundaries by LTSLM. We observe on one hand fairly homogeneous low- and high-resistance states, consistent with fully parallel and antiparallel orientation of the magnetization of the LCMO electrodes at the GB, respectively. As LTSLM measures locally dR/dT , it allows to reconstruct and compare the T dependence of both, the manganite film and GB resistance within a single bridge containing a GB. Hence, LTSLM, if combined with integral magnetotransport measurements, may provide important information for the understanding of low-field TMR effects in manganites. Finally, we have also detected nontrivial intermediate states where the magnetization inside of one of the LCMO films has flipped. For such situations, LTSLM is a powerful tool, as it directly images the quantity of interest (magnetoresistance) and its dependence on magnetic domain formation, which is important for any MR element. As LTSLM does not rely on smooth or reflective surfaces, this technique may thus provide important insight into the detailed behavior not only of manganite grain boundaries, but also of many other magnetoresistive devices.

We thank M. Peschka, R. P. Huebener, M. Fischer, P. Mühlshlegel and T. Schwarz for their contributions to the development of the laser microscope. This work was supported by the Deutsche Forschungsgemeinschaft.

[1] J. M. D. Coey and M. Viret, Adv. Phys. **48**, 167 (1999).
 [2] R. von Helmolt *et al.*, Phys. Rev. Lett. **71**, 2331 (1993).

[3] S. Jin *et al.*, Science **264**, 413 (1994).
 [4] H. Y. Hwang *et al.*, Phys. Rev. Lett. **77**, 2041 (1996).

- [5] A. Gupta *et al.*, Phys. Rev. B **54**, R15629 (1996).
- [6] N. D. Mathur *et al.*, Nature **390**, 266 (1997).
- [7] G. A. Prinz, Science **282**, 1660 (1998).
- [8] J. E. Evetts *et al.*, Phil. Trans. Roy. Soc. A **356**, 1593 (1998).
- [9] R. Gross *et al.*, J. Magn. Magn. Mater. **211**, 150 (2000).
- [10] A. Glaser and M. Ziese, Phys. Rev. B **66**, 094422 (2002).
- [11] J. S. Moodera and G. Mathon, J. Magn. Magn. Mater. **200**, 248 (1999).
- [12] H. Sun *et al.*, Phys. Rev. B **68**, 054413 (2003).
- [13] C. Höfener *et al.*, Europhys. Lett. **50**, 681 (2000).
- [14] F. Guinea, Phys. Rev. B **58**, 9212 (1998).
- [15] M. Ziese, Phys. Rev. B **60**, R738 (1999).
- [16] K. Steenbeck *et al.*, Appl. Phys. Lett. **73**, 2506 (1998).
- [17] J. B. Philipp *et al.*, Phys. Rev. B **62**, R9248 (2000). See also Phys. Rev. B **66**, 224417 (2002).
- [18] M. G. Blamire *et al.*, Appl. Phys. Lett. **82**, 2670 (2003).
- [19] R. Gunnarsson *et al.*, Phys. Rev. B **69**, 054413 (2004).
- [20] M. Julliere, Phys. Lett. **54A**, 225 (1975).
- [21] J.-H. Park *et al.*, Nature **392**, 794 (1998).
- [22] J. Z. Sun *et al.*, Appl. Phys. Lett. **69**, 3266 (1996).
- [23] M. Viret *et al.*, Euro. Phys. Lett. **39**, 545 (1997).
- [24] M.-H. Jo *et al.*, Phys. Rev. B **61**, R14905 (2000).
- [25] N. K. Todd *et al.*, J. Appl. Phys. **85**, 7263 (1999).
- [26] P. M. Shadrin and Y. Y. Divin, Physica C **297**, 69 (1998).
- [27] P. X. Zhang, W. K. Lee, and G. Y. Zhang, Appl. Phys. Lett. **81**, 4026 (2002).
- [28] Q. Y. Jin *et al.*, Phys. Rev. Lett. **72**, 768 (1994).
- [29] This is due to the half-metallicity of the doped manganites and the nature of the transport processes across the disordered grain boundary region, which have been discussed extensively in Refs. 8,9,13,15,17.